

Scientific paper

Separation of Biogas Components with Single Wall Carbon Nanotubes: a GCMC Simulation

Saeid Yeganegi* and Fatemeh Gholampour

Department of Physical Chemistry, Faculty of Chemistry, University of Mazandaran, Babolsar, Iran

* Corresponding author: E-mail: yeganegi@umz.ac.ir;
Tel & Fax: +98-112-5342350

Received: 22-04-2012

Abstract

Biogas is a green energy source that mainly contains CH₄, CO₂, traces of H₂S and fractions of H₂O vapor. One of the effective methods in biogas treatment from its pollutants is adsorptive separation. Here, enrichment of methane using (10, 10) and (6, 6) carbon nanotubes (CNTs) in modelled biogas consisting CH₄, CO₂ and H₂S is studied. Simulations were carried out using Grand Canonical Monte Carlo (GCMC) method. Adsorption isotherms obtained at various temperatures and pressures for two single wall carbon nanotubes (SWCNTs). To quantify the separation ability of the nanotubes the adsorptive separation factors for H₂S/CH₄ and CO₂/CH₄ were calculated. For studying temperature effect, simulations at two (0.1 and 1 MPa) pressures and four temperatures: 288, 298, 318 and 338 K have been performed. In all studied conditions, CO₂ is preferentially adsorbed by CNTs. Results have shown that the two separation factors are considerable, particularly for (10, 10) CNT. Additionally, the adsorption and selectivity behaviour of studied gases were considered in (6,6), (8,8) and (10,10) CNT hexagonal bundles for comparison. The results for single nanotubes were confirmed with the bundles. Hence, despite lower concentration of CO₂ than CH₄ and trace amount of H₂S in biogas, they can be separated from methane effectively by CNTs as adsorbents. Our results showed that the CNTs can be remarkable tools in methane separation from biogas.

Keywords: Biogas; adsorption; SWCNT; hydrogen sulphide; methane

1. Introduction

Biogas is a green renewable energy source that attracted more attention in recent years because of its high potential being as an environmentally friendly fuel. Raw biogas contains 55–65% methane (CH₄), 30–45% carbon dioxide (CO₂), traces of hydrogen sulphide (H₂S) and fractions of water vapor.¹ Methane enrichment from sour gases such as H₂S and CO₂ has a significant effect on biogas applicability. After elimination of biogas pollutants, it can be a suitable substitute for natural gas.

Biogas treatment involves aerobic biological, catalytic or oxidative processes and adsorptive separation processes, the later one exploiting various types of adsorbents, is also widespread. Adsorptive technologies with economical and technical efficiencies are used in many applications such as gas treatment. Among them, nanoporous carbon adsorbents recently have been applied widely in the field of gas separation² due to their advantages such as high selectivity and stability at high temperatures and

pressures. In this work we used CNTs as representatives of the channels and pore mouths of nanoporous carbon adsorbents.

A few experimental studies have been reported on the separation of biogas impurities. Harasimowicz and his coworkers¹ used capillary module for H₂S and CO₂ removal from biogas with a polyimide membrane. Esteves et al.³ analyzed natural gas and biogas components adsorption on activated carbon. Orme et al.⁴ used supported polyphosphazene membranes for measuring permeability and separation of H₂S mixture with light gases such as H₂, Ar, N₂, O₂, CH₄, and CO₂. Experimental analysis of biogas separation with adsorbents is difficult because of the toxicity of its components, expensive laboratorial equipment and difficulties in detecting and determining the behavior of molecules inside nanopores of adsorbent. Molecular simulations are powerful tools to survey adsorption and transport phenomena in nanopores. Some researchers performed this method to prospect ability of several adsorbents in biogas components separation. Cosoli et al.^{1,6}

performed GCMC and MD simulations to study hydrogen sulphide removal from biogas streams by different zeolites such as FAU, LTA and MFI types. Their results suggested that hydrophilic zeolites are more indicated for H₂S adsorption. Ahmad and coworkers⁷ studied capillary condensation method for separation of hydrogen sulfide from methane by nanoporous membranes.

To our knowledge there aren't any reported theoretical or experimental data about separation of biogas components using carbonaceous adsorbents such as CNTs. This promoted us to simulate and examine the ability of these materials in separation of CH₄ from other biogas components by grand canonical Monte Carlo (GCMC) simulation.

2. Modeling

The armchair (10, 10) and (6, 6) CNTs corresponding to the diameters of 1.356 and 0.814 nm respectively, were used in this work. The CNTs are treated as rigid nanotubes and adsorbate-nanotube interactions were calculated by summing over pairwise contributions between adsorbate and carbon atoms of the nanotube. The lengths of nanotubes were held fixed at 5 nm.

Many different potential models are available for CO₂. Huang et al.⁸ compared simulation of CO₂ adsorption inside (6,6) and (10,10) CNTs of spherical Ravikovitch⁹ model with three site EPM2 model of Harris and Yung¹⁰ and observed that their results are qualitatively and quantitatively similar. Thus we have chosen the spherical model of Ravikovitch for lower computational cost. The CH₄ molecule represented as a Lennard-Jones sphere according to the OPLS parameterization by Grade et al.¹¹. The carbon atoms of nanotube were assumed to be Lennard-Jones spheres and the H₂S was modeled as one LJ center and four polar sites, according to Kristof and Liszi¹². In this model the Lennard-Jones plus polar site located in the experimentally position of sulfur nucleus. Other three polar sites are located on two Hydrogen atomic nuclei and at a point on the bisector of the H-S-H angle. The intermolecular potential parameters used in this work are shown in Table 1.

3. Simulation Details

A GCMC simulation of adsorption performs at constant temperature, chemical potential and volume. The GCMC algorithm for a molecular fluid consists of four types of moves: translation, rotation, creation, and deletion of particles.¹³ Because it allows a direct calculation of the phase equilibrium between a gas phase and an adsorbate phase, this type of simulation had been used widely for the simulation of adsorption. To hold the chemical potentials of all components fixed, the framework must be in open contact with an infinite bulk gas phase at a given temperature. This reservoir is completely described by temperature and fugacity of all components, and does not have to be simulated explicitly. In each pressure, partial pressures of biogas components are calculated using their mole fractions. Biogas component's mole fractions was assumed to be 68% CH₄, 30% CO₂ and 2% H₂S, according to the reported experimental work by Harasimowicz.¹ The reservoir chemical potentials for each component are related to the fugacity (or partial pressure) of the components. For relating the reported pressure and fugacities we used virial equation of state. At least 2×10^7 productive Monte Carlo steps have been performed under 3D periodic boundary conditions. The cutoff distance for calculating LJ interactions was 12 Å. The Lorentz-Berthelot¹⁴ mixing rule was used for the cross-term LJ parameters. The coulombic interactions were accounted for by Ewald summation technique.¹⁵ Six temperatures from 288 up to 338K and eight pressures from 0.1 to 30 MPa were chosen to investigate the effects of the temperature and pressure on the adsorption behavior of biogas components in SWCNTs.

4. Results and Discussion

At first we simulated the pure gas adsorption in (10, 10) CNT to obtain the heats of adsorption and also the corresponding adsorption isotherms.

Heats of adsorption or isosteric heat of adsorption defined as the enthalpy change of the system when the gas molecules transfer from their state in the bulk phase to the

Table 1. The LJ parameters and site charges that were used in the simulations.

Atom (molecule)	position(Å)		σ (Å)	ϵ/k_B (K)	q(e)	Ref.
	y	x				
CH ₄	0	0	3.730	147.99	0	12
CO ₂	0	0	3.454	235.90	0	12
S (H ₂ S)	0	0	3.730	250	0.4	9
H1 (H ₂ S)	0.934	0.931	0	0	0.25	
H2 (H ₂ S)	-0.934	0.931	0	0	0.25	
M (H ₂ S)	0	0.186	0	0	-0.9	
C (CNTs)	0	0	3.550	35.26	0	12

adsorbed state. The isosteric heat of adsorption (q_{st}) can be calculated by a Clausius–Clapeyron like equation as

$$q_{st} = RT^2 \left(\frac{\partial \ln P}{\partial T} \right)_\theta \quad (1)$$

Where R is the universal gas constant and θ is the fraction of occupied sites of adsorbent. It should be noted that although there are some approximations to attain equation 1 (adsorption reversibility, the ideal behavior of bulk gas and negligible molar volume of adsorbed gases) these simplifications have negligible effect on the survey of q_{st} . This equation is not straightforward to realize q_{st} by GCMC simulations, therefore we have used the direct equation

$$q_{st} = RT - \left(\frac{\partial U}{\partial N_{ad}} \right)_{T,V} \quad (2)$$

In this equation N_{ad} is the number of adsorbed molecules and U is the total energy of the system that consists of adsorbate-adsorbate and adsorbate-adsorbent both coulombic and noncoulombic interactions. To achieve equation (2) the assumptions of the equation (1) have been used, additionally it is assumed that internal degrees of freedom of the adsorbate molecules do not change appreciably upon adsorption.^{16–18}

In this work the adsorbate molecules are assumed to be rigid interaction sites, therefore the direct addition of gas-gas and gas-CNT interaction energies will give the total energy of adsorption. Fig. 1 shows CH_4 - CH_4 and CH_4 -(10,10) CNT interaction energies and sum of them as a function of the number of gas molecules at 298 K.

The points are simulation results and solid lines are least square fittings. The same simulations have been performed for CO_2 and H_2S adsorption in (10, 10) CNT but we don't present them here for brevity. The dependence of

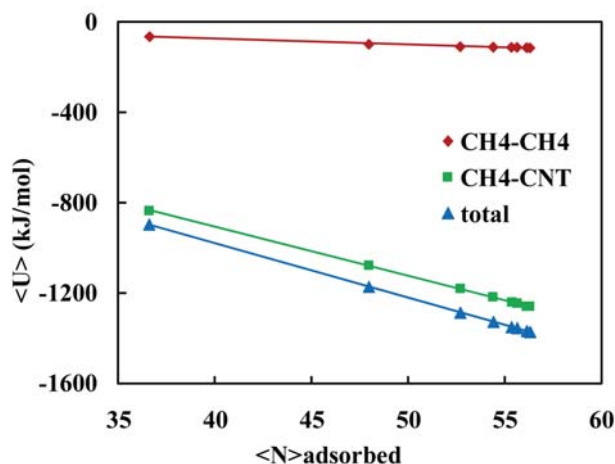


Fig. 1. Adsorption energy components versus number of adsorbed CH_4 molecules in (10, 10) CNT at 298K. Solid lines are least square fits to linear equations.

energies to loading is almost linear. The gas-CNT contribution to the adsorption energy is much larger than gas-gas interaction. The average isosteric heats of adsorption estimated as 26.59, 33.28 and 44.13 kJ/mol for CH_4 , CO_2 and H_2S respectively in (10, 10) CNT at 298 K. The calculated isosteric heats of adsorption show that the adsorption energies of H_2S and CO_2 are larger than CH_4 . This can be described in terms of greater interaction strength parameters for CO_2 and H_2S compared to CH_4 one's. To the best of our knowledge, there aren't any reported experimental data about the heats of adsorption of biogas components in simple SWCNTs. Swanat et al.¹⁹ were reported the values of 17 and 29 kJ/Mol for the heats of CH_4 and CO_2 adsorption in synthesized horn shaped CNTs. Anderson and coworkers²⁰ were attained the values of 26.0 ± 0.6 for CO_2 and 19.1 ± 0.9 for CH_4 adsorption in a NPC. So, our results are in agreement with those reported for NPC-s. Also our calculated q_{st} for CO_2 and CH_4 adsorption in CNTs were in agreement with the reported heats of adsorption of the same molecules in hypothetical C_{168} schwarzite.²¹ In addition, the trend of heats of adsorption in (10,10) CNT is in agreement with observed trends in zeolites.⁵

Second, we calculated the adsorption isotherms of the pure components of biogas at room temperature inside the (10, 10) CNT. In Fig. 2 the adsorption isotherms of pure gas components have shown as loadings versus pressure.

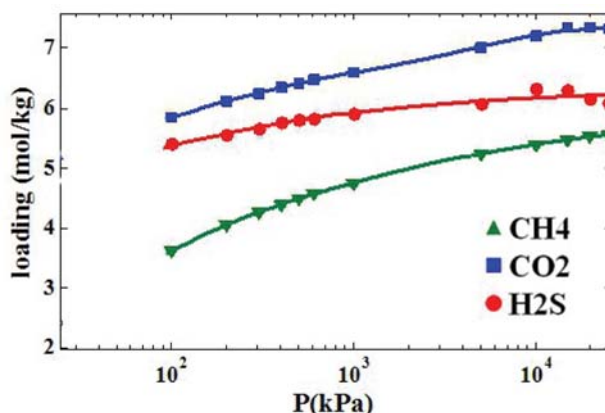


Fig. 2. Adsorption isotherm of pure biogas components in (10, 10) CNT at 298 K. Solid lines are fits to the dual-site Langmuir-Freundlich equation.

The loading is defined as the average number of molecules inside the nanotube per one kilogram of the nanotube. Pure gas loadings decreases in order of $\text{CO}_2 > \text{H}_2\text{S} > \text{CH}_4$ which is not unexpected if one considers the interaction sites potential parameters of three molecules. The potential well depth of CO_2 and H_2S are deeper than the CH_4 and then they attracted more by CNT's carbon atoms. Also the isosteric heats of adsorption of H_2S and CO_2 are larger than the CH_4 . The loading of CO_2 is greater than the H_2S at all studied pressures. At high pressures the loading

of CO₂ increases nearly linear nevertheless the loading of H₂S at higher pressures became constant and then decreased. The CO₂ molecule has a smaller diameter than H₂S thus adsorption of a fixed number of CO₂ molecules occupies a smaller number of adsorbent sites than the adsorption of the same number of H₂S molecules. The adsorption isotherms in Fig. 2 are approximately ascending with pressure for all three molecules although adsorption of CH₄ increases more rapidly than the others. The CH₄ and CO₂ adsorption amounts are in agreement with the experimental data reported in the same conditions in SWCNTs with Lithoxoos et al.²². The pure CO₂ adsorption is in close agreement with the results of Huang and coworkers.⁸ The adsorption isotherms of CO₂ and CH₄ are also in agreement with the reported loadings in hypothetical Schwarzite (C₁₆₈) model of nanoporous carbon membranes at room temperature.²¹

We have used the dual site Langmuir-Freundlich (DSLFL) equation to fit the adsorption isotherms of pure gases.

$$N^0(f) = \frac{N_1 K_1 f^{n_1}}{1 + K_1 f^{n_1}} + \frac{N_2 K_2 f^{n_2}}{1 + K_2 f^{n_2}} \quad (3)$$

In this equation f is the fugacity of bulk gas that has been related to the chemical potential of the system, $N^0(f)$ is the relevant loading of adjusted fugacity. N_i is the maximum loading in site i , k_i is the affinity constant and n_i is representative of deviation from Langmuirian adsorption.^{16,23,24} The solid lines in Fig. 2 shows the fitted isotherms and Table 2 represents the fitted parameters and regression coefficients of the fitted curve.

Table 2. The fitted parameters of dual-site Langmuir-Freundlich equation to simulated adsorption isotherms of pure biogas components inside (10, 10) CNT.

parameter	adsorbate		
	CH ₄	CO ₂	H ₂ S
N_1	1.941	9.855	8.139
K_1	0.021	0.357	0.726
n_1	0.448	0.128	0.109
N_2	4.402	2.110	0.973
K_2	0.113	0.670	14.210
n_2	0.724	0.657	4.783
R^2	0.9999	0.9944	0.9636

Attending fitted DSLFL curves and lower regression coefficients of H₂S loadings, it is clear that H₂S loadings are weaker converging to the DSLFL equation with respect to CH₄ and CO₂. Comparison with ideal adsorption, CH₄ adsorption with nearer n_1 to 1 is predicted to be more langmuirian than the other gases. The total capacity for CO₂ adsorption (N_1+N_2) is more than H₂S and that for CH₄ is the lowest, this order observed also in the loading

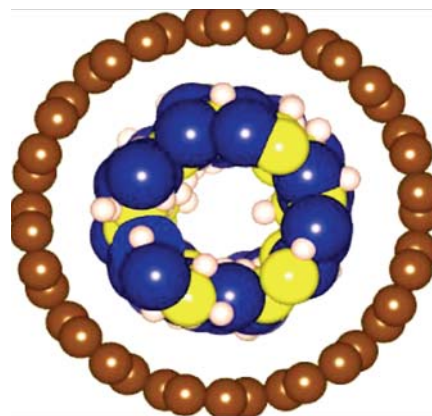


Fig. 3. Snapshot of last configuration of biogas components in (10, 10) CNT at 298 K.

amounts of pure gases. Greater adsorption amounts of H₂S can be resulted from greater affinity constant for H₂S. These parameters in comparison with the reported DSLFL parameters for C₁₆₈ in ref.²¹ illustrates that both nanopores have higher adsorption capacity for CO₂ than CH₄. Also adsorption in C₁₆₈ better imitates from the Langmuir adsorption model than the (10, 10) CNT.

We simulated biogas mixture inside a (10, 10) SWCNT to shed light on the adsorption behavior of biogas components in the mixture. Fig. 3 shows a snapshot of adsorbed particles in (10, 10) CNT derived from the last configuration of a normally terminated simulation run.

It is apparent that the adsorbed molecules, configured as a tube inside the CNT. The attraction between the fluid's molecules and CNT's carbon atoms dominates the repulsion between gas molecules.

Fig. 4 shows adsorption isotherms for components of biogas in (10,10) CNT at 298 K

The symbols are our data while lines are set to guide the eye. In biogas mixture, CO₂ and H₂S have been more adsorbed than CH₄ while CO₂ has been adsorbed more than H₂S in all pressures. The larger CO₂ adsorption than

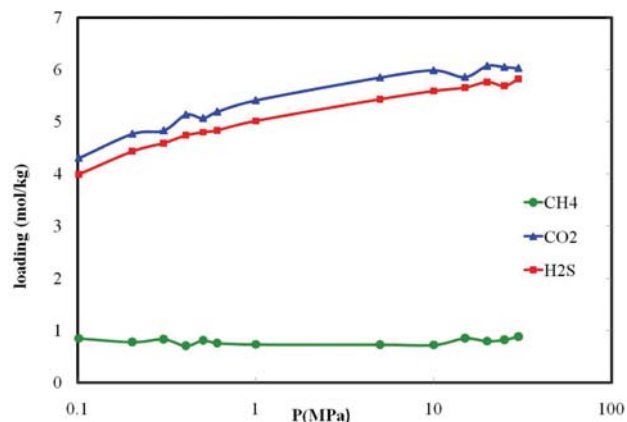


Fig. 4. Adsorption isotherm of biogas mixture in (10, 10) CNT at 298 K. Solid lines are guides to the eye.

the other biogas components is also reported in a study of adsorption of biogas components in NaY, MFI and LTA types of zeolites.⁵ It is interesting that the adsorption of CH₄ is much lower than the other components although its mole fraction in bulk phase is much larger than the other components. At low pressures, the loadings of CO₂ and H₂S increase rapidly with pressure however CH₄'s loading decreases slightly. Increasing the bulk pressure higher than 5 MPa has little effect on the adsorption of biogas components. However, at 15 MPa the adsorption of CO₂ decreases and then increases again. For the pressures greater than 15 MPa the loadings of CO₂ and H₂S oscillate slightly but they become very close at the highest pressure again.

To study the effect of temperature on the adsorption of biogas components, adsorption isotherms have been obtained at four temperatures (288, 298, 318, and 338 K) and two pressures (0.1 and 5 MPa). Fig. 5 illustrates loadings as a function of temperature for two pressures, 0.1 and 5 Mpa.

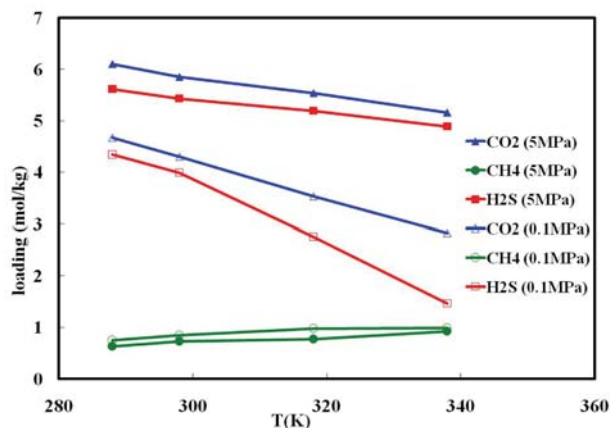


Fig. 5. Loading of biogas mixture versus temperature for (10, 10) CNT at two pressures. Unfilled symbols used for 0.1 Mpa and filled symbols for 5 Mpa. Solid lines are guides to the eye.

The loadings of CO₂ and H₂S decrease with temperature whereas at lower pressure the loading decreases more than higher pressure. This finding is in agreement with the generally accepted behavior of physisorption phenomena. However, the loading of CH₄ increases slightly with temperature which can be related to the releasing of more adsorption sites due to the adsorption diminishing of CO₂ and H₂S molecules. In Fig. 5, the adsorption of H₂S at the lower pressure decreases rapidly with temperature, however for the highest considered temperature it is near the CH₄'s adsorption.

Adsorption selectivity of component *i* versus *j* defined as:

$$S_{ij} = \left(\frac{x_i}{x_j} \right) \left(\frac{y_j}{y_i} \right). \quad (4)$$

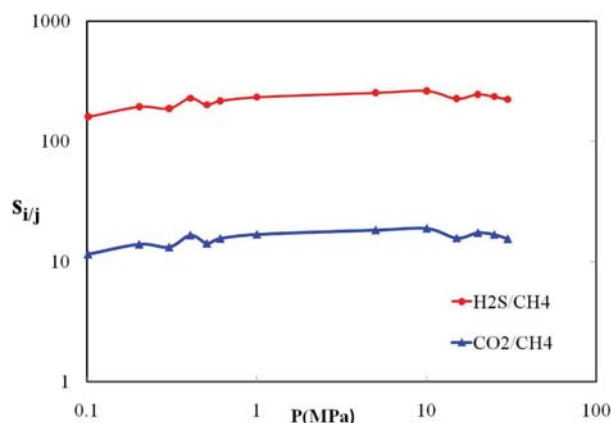


Fig. 6. Adsorption selectivity versus the pressure of biogas components in (10, 10) CNT at 298 K. Solid lines are guides to the eye.

Where x_i , y_i are the mole fractions of component *i* in the adsorbed and bulk phase, respectively.^{21,25} Considering separation capacity of (10, 10) CNT, H₂S/CH₄ and CO₂/CH₄ adsorption selectivity has been calculated. Fig. 6 shows H₂S/CH₄ and CO₂/CH₄ selectivity of (10, 10) CNT at room temperature as a function of pressure.

The H₂S/CH₄ selectivity is much higher than CO₂/CH₄ except at 0.1 Mpa, once the H₂S/CH₄ selectivity is greater than 200. Selectivity of H₂S/CH₄ for pressures up to 10 MPa increases and it comes to 260 and afterwards it oscillates slightly. Nevertheless, large amount of H₂S/CH₄ separation factor (near 200) is representing that CNTs could be a useful tool for biogas separation or methane enrichment from its toxic and corrosive component: H₂S. This result is comparable with results of zeolitic adsorbents that reported with Cosoli et. al.⁵ This range of separation factors is higher than the hydrophobic NaY or LTA zeolites but it is lower (in some cases nearer) than hydrophilic MFI type zeolites. Though the CO₂/CH₄ selectivity was much lower than those of H₂S/CH₄; but they

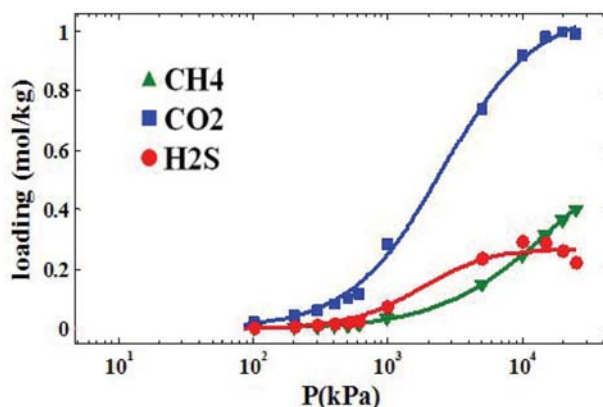


Fig. 7. Adsorption isotherm of pure biogas components in (6, 6) CNT at 298 K. Solid lines are fits to the dual-site Langmuir-Freundlich equation.

are greater than 10. It is demonstrating that although CH_4 has higher partial fugacity than CO_2 and H_2S in bulk phase but the (10, 10) CNT adsorbs them more than CH_4 , therefore (10,10) CNT has a great potential as a methane purification adsorbent from biogas.

To study the pore size effect on the adsorption of biogas components; we calculated adsorption isotherms of pure CH_4 , CO_2 and H_2S and biogas mixture in a (6, 6) SWCNT. The simulation conditions are similar to those for (10, 10) CNT. Because of less adsorption of pure gases in (6, 6) CNT, we didn't calculate q_{st} for this nanopore. Fig. 7 shows adsorption isotherms for pure components of biogas in (6, 6) CNT at 298 K and pressures from 0.1 to 30 MPa.

The adsorption amounts in (6, 6) CNT are much lower than those for (10, 10) CNT, as expected. Pure CO_2 adsorption isotherm is in agreement with the reported adsorption isotherm of spherical and EPM2 model of CO_2 in (6, 6) CNT at 293K.¹⁰ At pressures up to 15 Mpa CH_4 's adsorption was lower than that of H_2S but for higher pressures this order has been inverted and loading of CH_4 increases rapidly. This can be related to the smaller size of methane molecules. The pure CH_4 adsorption curve is ascendant in all of pressures while pure CO_2 and H_2S loadings are decreasing respectively after 20 and 15 Mpa.

The Solid lines in Fig. 7 shows fitted data to DSLF equation. Table 3 illustrates the fitted parameters using DSLF equation and the regression coefficients of fitting.

Table 3. The fitted parameters of the dual-site Langmuir Freundlich equation to simulated adsorption isotherms of pure biogas components inside (6, 6) CNT.

parameter	adsorbate		
	CH_4	CO_2	H_2S
N_1	0.217	0.9885	1.724
K_1	4.998×10^{-5}	4.455×10^{-5}	8.513×10^{-5}
n_1	1.092	1.109	0.5488
N_2	0.00179	7.425×10^{-4}	0.01041
K_2	0.001733	1.907×10^{-7}	0.005973
n_2	1.07×10^{-5}	1.212×10^{-7}	0.05998
R^2	0.9995	0.9994	0.9326

The Smaller N_1 and N_2 parameters of DSLF equation for (6,6) CNT with respect to (10, 10) CNT represents lower adsorption capacity of (6, 6) CNT. Also a comparison of K_i constants between two CNTs confirms that the (6, 6) CNT has a lower affinity for adsorption of gas molecules than the larger CNT. The fugacity powers (n_i) indicate deviation from the langmuirian adsorption then one can say that the site 1 for (6,6) CNT obeys the ideal adsorption model better than the site1 of the (10, 10) CNT. The adsorption in site 2 is very deviant from Langmuir equation. Inspecting N_i and K_i parameters for three

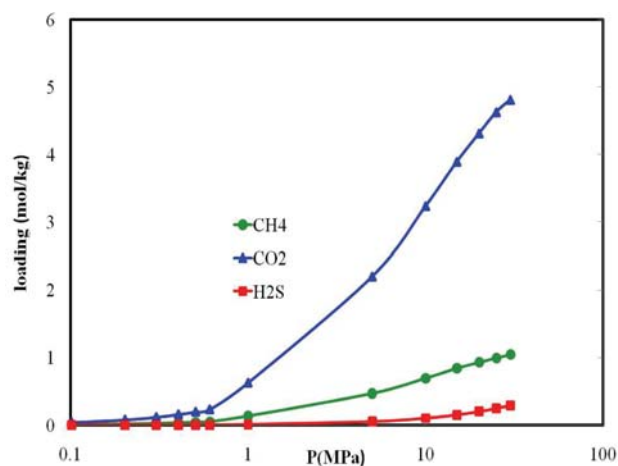


Fig. 8. Adsorption isotherm of biogas mixture in (6, 6) CNT at 298 K. Solid lines are guides to the eye.

molecular components shows that saturation capacity and adsorption affinity for adsorption of H_2S in (6, 6) CNT is greater than the other biogas components and that for CH_4 is the lowest.

Fig. 8 shows adsorption isotherms of biogas mixture components at 298K in (6, 6) CNT.

Unlike the (10, 10) CNT, where the adsorption amount of CH_4 was the lowest, here adsorption of H_2S is the lowest one. The loading of CH_4 and H_2S were very low except at higher pressures which is a consequence of molecular diameters. At low pressures, for both pure and biogas mixture components; the loadings of all components are very low and close to each other which is reasonable if one compare diameter of the tube and molecules. Also in both pure and biogas mixture CO_2 adsorption increases rapidly with pressure. In conclusion adsorption inside thin CNTs affected mainly by the molecular diameter, the smaller molecules adsorbs more.

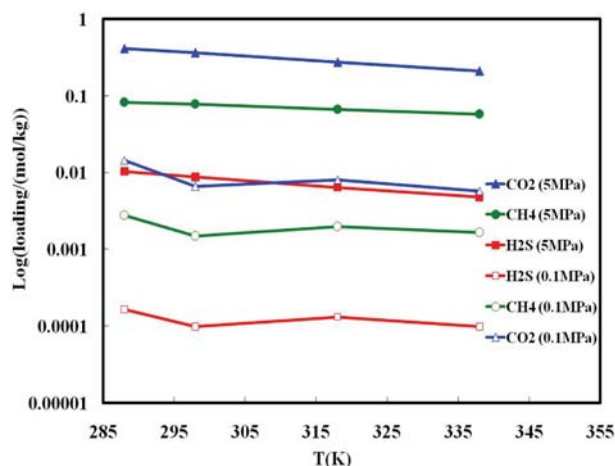


Fig. 9. Loading of biogas components versus temperature for (6, 6) CNT at two pressures. Unfilled symbols used for 0.1 Mpa and filled symbols for 5 Mpa. Solid lines are guides to the eye.

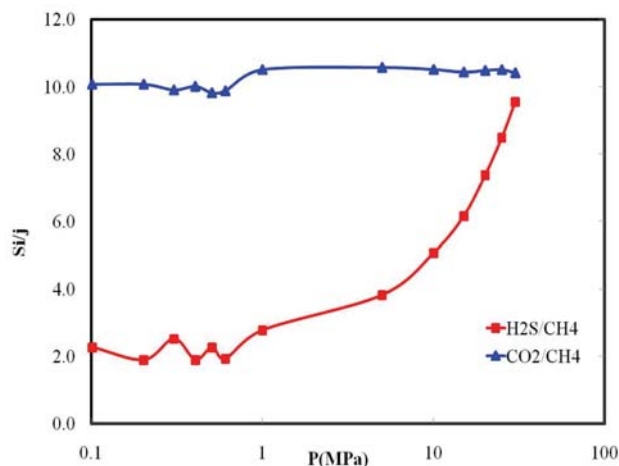


Fig. 10. Adsorption selectivities of biogas components in (6, 6) CNT at 298 K. Solid lines are guides to the eye.

We then have surveyed the temperature effect on the biogas adsorption inside the (6, 6) CNT. Fig. 9 shows adsorption of biogas components in (6, 6) CNT at 0.1 and 5 MPa of pressure and temperatures range from 288 to 338 K.

In (6, 6) CNT similar to the (10, 10) CNT, CO_2 adsorption was dominant but unlike (10, 10) CNT at all studied temperatures, the adsorption of H_2S was lower than others. Increasing the temperature causes a small diminish of loadings for all components when the CH_4 adsorption in (10, 10) CNT was increasing with temperature. In comparison with adsorptions in (10, 10) CNT decreasing of loadings with temperatu-

re was much smaller. For pressure 0.1 MPa when temperature changes from 288 to 298 K all of the loadings decreased.

We have calculated separation factors of biogas components for (6, 6) CNT applying the calculated loadings. Fig. 10 shows $\text{H}_2\text{S}/\text{CH}_4$ and CO_2/CH_4 separation factors at 298 K versus bulk pressure.

The adsorption selectivity of CO_2/CH_4 is about 10 and is similar to that of (10, 10) CNT but $\text{H}_2\text{S}/\text{CH}_4$ selectivity is very low when it compared to same selectivity inside (10, 10) CNT and regardless of its increasing with pressure it couldn't achieve the selectivity range of (10, 10) CNT or that of CO_2/CH_4 . Nevertheless CO_2/CH_4 and $\text{H}_2\text{S}/\text{CH}_4$ separation factors were larger than 1 show that the (6, 6) CNT, regardless of its low loading capacity, yet prefers biogas impurities for separation from methane.

To validate our model of nanotube and study whether the use of only one nanotube for the simulations affects the observed trends in the system, we have perfor-

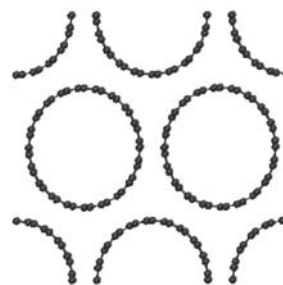


Fig. 11. Simulation cell for hexagonal CNT bundle.

Table 4. Loading amounts (mol/kg) of pure gases in CNT bundles at $T = 298$ K and three selected pressures.

Loading	100kpa			1000kpa			5000kpa		
	CH4	CO2	H2S	CH4	CO2	H2S	CH4	CO2	H2S
(6,6)	1.790	1.960	1.856	1.849	2.027	1.856	1.860	2.116	1.856
(8,8)	1.585	2.941	2.73	2.315	3.793	3.281	2.728	4.102	3.254
(10,10)	1.652	3.8097	3.6177	3.643	5.638	5.103	4.347	6.546	5.275

Table 5. Loading amounts (mol/kg) of biogas mixture in CNT bundles at $T = 298$ K and three selected pressures.

Loading	100kpa			1000kpa			5000kpa		
	CH4	CO2	H2S	CH4	CO2	H2S	CH4	CO2	H2S
(6,6)	0.470	0.829	0.556	0.608	0.739	0.516	0.706	0.733	0.466
(8,8)	0.557	1.422	0.332	0.477	2.533	0.230	0.567	2.467	0.562
(10,10)	0.937	1.399	0.335	1.115	2.938	0.691	1.344	3.43	0.569

Table 6. $\text{H}_2\text{S}/\text{CH}_4$ and CO_2/CH_4 Selectivities in CNT bundles at $T = 298$ K and three selected pressures.

	100kpa		1000kpa		5000kpa	
	$S_{\text{H}_2\text{S}/\text{CH}_4}$	$S_{\text{CO}_2/\text{CH}_4}$	$S_{\text{H}_2\text{S}/\text{CH}_4}$	$S_{\text{CO}_2/\text{CH}_4}$	$S_{\text{H}_2\text{S}/\text{CH}_4}$	$S_{\text{CO}_2/\text{CH}_4}$
(6,6)	40.22	4.000	28.85	2.753	22.45	2.353
(8,8)	20.28	5.787	16.394	12.036	33.700	9.849
(10,10)	12.156	3.384	21.071	5.972	14.394	5.784

med simulations on a hexagonal bundle of the CNTs. The relevant simulation cell is shown in Fig. 11.

The adsorptions of pure components and a mixture of biogas in the bundles of (6,6), (8,8) and (10,10) CNTs at three pressures and the temperature of 298K were simulated. The results are represented in Tables 4 and 5 respectively.

As it is shown in table 4 the adsorption amounts of pure gases in (6,6) CNT bundle show a similar trend as the adsorption amounts in an isolated CNT, For (10,10) bundle, the loadings are slightly lower than those of a single CNT. But in both cases the loading values for bundles are in the same order of magnitude of the corresponding single CNT and the trends are reserved. In table 5 the calculated loading of components of the biogas mixture in (6,6) bundle is very low when compared to the other bundles, this observation is inline with that observed in single CNTs. The adsorption amount of the components of the biogas mixture in (10,10) bundle is lower than that of a (10,10) CNT. Alike pure gas simulations, using bundles of CNTs don't change the trends of biogas component loadings, so that the adsorption of CO₂ is dominant in all cases. On the other hand, with increasing tube diameters, the loadings increase either for pure gases or biogas mixture in all cases. Table 6 represents the H₂S and CO₂ selectivities of CNT bundles with respect to CH₄ in modeled biogas mixture. From table 6 one can say that the H₂S/CH₄ selectivity in (6,6) bundle at the pressure of 100kpa achieves its greatest value: 40.22. In this case increasing the pressure will decrease the selectivities. So, the selectivity trend in (6,6) bundle is relatively different from the (6,6) CNT. For (10,10) bundle, the H₂S/CH₄ and CO₂/CH₄ selectivities are higher than 10 and 3 respectively. In total the selectivities of (10,10) bundle increase with pressure up to 1000kpa and decreases afterwards. Since the calculated loadings in CNT bundles have revealed the same trend as single CNT, one can say that using one nanotube in a unit cell doesn't induce sensible change in the adsorptive behavior of studied gases in CNTs.

5. Conclusions

Grand canonical Monte Carlo simulation of pure CH₄, CO₂, H₂S and biogas mixture adsorption were carried out in (10, 10) and (6, 6) CNTs representative of nanoporous adsorbent pores. Isothermic heats of adsorption estimated from simulation results for pure gas adsorption in (10, 10) CNT have shown that the adsorption energy of H₂S was larger than CO₂ and CH₄ while CH₄ has the smallest heat of adsorption. This is expectable if one considers the adsorbate-adsorbent interaction parameters. Adsorption isotherms at the 298 K show that both CNTs have adsorbed CO₂ more dominantly.

In (10, 10) CNT, pure CO₂ and CH₄ adsorption extents are consistent with available experimental and simu-

lation data. The parameters of the fitting of the calculated loadings of pure gases in both CNTs to the DSLF equation of state showed that CH₄ adsorption is more langmuirian than the other gas components. Also H₂S affinity for adsorption on studied CNTs is more than the same constants for CO₂ and CH₄. In (10, 10) CNT, adsorption of CH₄ in the biogas mixture is very low and is not affected by pressure but in (6, 6) CNT, CH₄ loadings are more than the other gases. To study the temperature effect on adsorption behavior, we have done the simulation for 4 temperatures (288, 298, 318 and 338 K) and two pressures (0.1 and 5 MPa) in both CNTs. In both nanopores, CO₂ was adsorbed more than other components of biogas. In (10, 10) CNT for all temperatures and pressures, the adsorption of CH₄ was lower than H₂S whereas its bulk partial pressure was far greater which causes the H₂S/CH₄'s separation factor to become very high (about 200). In (6, 6) CNT, adsorption amount of H₂S in biogas mixture is lower than CH₄ but because of high bulk pressure of CH₄, the H₂S/CH₄ separation factor was greater than 1 and increased to 10 in higher temperatures. For comparison We used hexagonal arrays of CNTs and performed simulations at (6,6), (8,8) and (10,10) CNT bundles in three selected pressures. The results show the slightly different results but the same trends observed with the single studied CNTs.

We can say that CNTs with porosity of about 13 Å; can be a powerful biogas treatment tool, and lower porosities (about 8 Å) give weaker separation yield.

6. Acknowledgments

We thank the financial support of this work by university of Mazandaran.

7. References

1. M. Harasimowicz, P. Orluk, G. Zakrzewska-Trznadel, A. G. Chmielewski, *J. Hazard. Mater.* **2007**, *144*, 698–702.
2. J. C. Palmer, K. E. Gubbins, *Micropor. Mesopor. Mater.* **2012**, *154*, 24–37.
3. I. A. A. C. Esteves, M. S. S. Lopes, P. M. C. Nunes, J. P. B. Mota, *Sep. Purif. Technol.* **2008**, *62*, 281–296.
4. C. J. Orme, F. F. Stewart, *J. Membr. Sci.* **2005**, *253*, 243–249.
5. P. Cosoli, M. Ferrone, S. Pricl, M. Fermeiglia, *Chem. Eng. J.* **2008**, *145*, 86–92.
6. P. Cosoli, M. Ferrone, S. Pricl, M. Fermeiglia, *Chem. Eng. J.* **2008**, *145*, 93–99.
7. F. Ahmad, H. Mukhtar, Z. Man, B. K. Dutta, *Chem. Eng. Process.* **2008** DOI:10.1016/j.cep.2007.11.015.
8. L. Huang, L. Zhang, Q. Shao, L. Lu, X. Lu, Sh. Jiang, W. Shen, *J. Phys. Chem. C*, **2007**, *111*, 11912–11920.
9. P. I. Ravikovitch, A. Vishnyakov, R. Russo, A. V. Neimark, *Langmuir*, **2000**, *16*, 311–2320.

10. J. G. Harris, K. H. Yung, *J. Phys. Chem.* **1995**, *99*, 12021–12024.
11. A. Kalra, G. Hummer, S. Garde, *J. Phys. Chem. B*, **2004**, *108*, 544–549.
12. T. Kristof, J. Liszi, *J. Phys. Chem. B*, **1997**, *101*, 5480–5483.
13. M. P. Allen, D. J. Tildesley, *Computer Simulation of liquids*, Oxford University Press (New York), **1987**, pp. 110–135.
14. L. Xu, M. Sahimi, T. T. Tsotsis, *Phys. Rev. E*, **2000**, *62*, 6942.
15. R. J. Sadus, *Molecular Simulation of Fluids*, Elsevier (Amsterdam), **1999**.
16. J. Jiang, J. B. Klauda, S. I. Sandler, *Langmuir*, **2003**, *19*, 3512–3518.
17. J. Jiang, J. B. Klauda, S. I. Sandler, *J. Phys. Chem. B*, **2004**, *108*, 9852–9860.
18. Sh. Li, J. L. Falconer, R. D. Noble, *J. Membr. Sci.* **2004**, *241*, 121–135.
19. S. Y. Sawanta, R. S. Somania, H. C. Bajaja, S. S. Sharmab, *J. Hazard. Mater.* **2012**, 227–228, 317–326.
20. C. J. Anderson, W. Tao, J. Jiang, S. I. Sandler, G. W. Stevens, S. E. Kentish, *Carbon*, **2011**, *49*, 117–125.
21. R. Babarao, Zh. Hu, J. Jiang, Sh. Chempath, S. I. Sandler, *Langmuir*, **2007**, *23*, 659–666.
22. G. P. Lithoxoos, A. Labropoulos, L. D. Peristeras, N. Kanellopoulos, J. Samiosd, I. G. Economou, *J. Supercrit. Fluid*, **2010**, *55*, 510–523.
23. M. B. Sweatman, N. Quirke, *Langmuir*, **2001**, *17*, 5011–5020.
24. M. Heuchel, G. M. Davies, E. Buss, N. A. Seaton, *Langmuir*, **1999**, *15*, 8695–8705.
25. P. Kowalczyk, L. Brualla, A. Zywockinski, S. K. Bhatia, *J. Phys. Chem. C*, **2007**, *111*, 5250–5257.

Povzetek

Bioplin spada med »zelene« vire energije, ki vsebuje pretežno CH₄ in CO₂ ter v sledovih H₂S in H₂O. Za čiščenje bioplina se je kot zelo učinkovita izkazala metode absorptivne separacije. V tem delu smo v ta namen uporabili (10, 10) in (6, 6) ogljikove nanocevke (CNT) ter veleanonsko metodo simulacije MonteCarlo (GCMC). Izračunali smo adsorpcijske izoterme pri različnih temperaturah in tlakih za dve enostenski ogljikovi nanocevki (single wall carbon nano tubes, SWCNT) ter faktorje separacije za sisteme H₂S/CH₄ ter CO₂/CH₄. Izkazalo se je, da se pri vseh proučevanih primerih CO₂ preferenčno adsorbira na CNT, kar bi lahko uporabili tudi v praksi za čiščenje bioplina.